Detecting repetitive icequakes at Llaima volcano, Chile

Oliver D. Lamb [1,*], **Jonathan M. Lees** [1], **Luis Franco Marin** [2], **Jonathan Lazo** [2], **Andrés Rivera** [3], **Michael J. Shore** [1], **and Stephen J. Lee** [4]

[1] *Department of Geological Sciences, University of North Carolina at Chapel Hill, Chapel Hill, NC, USA*
[2] *OVDAS-Sernageomin, Chilean Geological Survey, Chile*
[3] *Departamento de Geografía, Universidad de Chile, Chile*
[4] *U.S. Army Research Laboratory/Army Research Office, Research Triangle Park, NC, USA*

Correspondence*:
O. D. Lamb
olamb@email.unc.edu

ABSTRACT

Glacially- and magmatically-derived seismic events have been noted to heavily overlap in characteristics, thus there exists the potential for false-alarms or missed warnings at ice-covered volcanoes. Here we present the first study to specifically target icequakes at an ice-covered volcano in Southern Chile. Two months of broadband seismic data collected at Llaima volcano in 2015 were analyzed in order to quantify, characterize, and locate glacially-derived seismic events at one of the most active ice-covered volcanoes in the region. We find over 1,000 repeating seismic events across 11 families, the largest of which contains 397 events. Approximate locations and characteristics of the largest families lead us to conclude that these events were derived from persistent stick-slip motion along the ice-rock interface at the base of a glacier near the volcano summit. These results have implications for future seismic monitoring at Llaima volcano and other ice-covered active volcanoes in the region.

Keywords: volcano-seismology, icequakes, Llaima volcano, monitoring, repetitive

RESUMEN

Se ha observado que los fenómenos sísmicos derivados de los glaciares y magmáticos se superponen en gran medida en las características, por lo que existe la posibilidad de que se produzcan falsas alarmas o de que se pasen por alto las alertas en los volcanes cubiertos de hielo. Aquí presentamos el primer estudio que apunta específicamente a los terremotos en un volcán cubierto de hielo en el sur de Chile. Se analizaron dos meses de datos sísmicos de banda ancha recolectados en el volcán Llaima en 2015 para cuantificar, caracterizar y localizar eventos sísmicos derivados de glaciares en uno de los volcanes cubiertos de hielo más activos de la región. Encontramos más de 1,000 eventos sísmicos repetidos en 11 familias, el más grande de los cuales contiene 397 eventos. Las ubicaciones y características aproximadas de las familias más grandes nos llevan a la conclusión de que estos eventos se derivaron de un movimiento persistente de stick-slip a lo largo de la interfase de la roca de hielo en la base de un glaciar cerca

de la cima del volcán. Estos resultados tienen implicaciones para el futuro monitoreo sísmico en el volcán Llaima y otros volcanes activos cubiertos de hielo en la región.

1 INTRODUCTION

For volcano monitoring organizations a fundamental goal is to assess whether changes in seismicity indicates impending intensification of volcanic eruptive activity. Earthquakes generated by magma movement beneath volcanoes are recorded across a wide range of waveform shapes and frequencies (Chouet and Matoza, 2013). Low-frequency earthquakes linked to volcanic activity are traditionally thought to be generated by the resonance of fluid-filled cracks (e.g. Chouet, 1996), but may also be linked to slow-rupture failure of magma or volcanic materials (e.g. Neuberg et al., 2006; Iverson et al., 2006; Bean et al., 2013). However, seismicity generated by glaciers can often resemble signals associated with fluid or magma transport within volcanoes (Weaver and Malone, 1976; West et al., 2010). There are multiple documented processes for generating seismicity around glaciers, including crevassing, ice-fall events, stick-slip motion at the base, hydrofracturing within the ice, and subglacial water flow (Podolskiy and Walter, 2016; Aster and Winberry, 2017). Most or all of these mechanisms have been documented or surmised to occur in case studies at multiple ice-covered volcanoes (Weaver and Malone, 1976; Métaxian et al., 2003; Caplan-Auerbach and Huggel, 2007; Jónsdóttir et al., 2009; Thelen et al., 2013; Allstadt and Malone, 2014).

Glacial signals are usually weak and therefore only recorded at stations close to the source (Weaver and Malone, 1976), but there are documented examples of glaciers producing earthquakes as large as magnitude 5 (Ekstrom et al., 2003) and/or being recorded at considerable distance from the source (e.g. Caplan-Auerbach and Huggel, 2007). Most cases of documented glacial signals describe a strong attenuation of higher frequencies between the source and receiver (Weaver and Malone, 1979; Métaxian et al., 2003; Thelen et al., 2013; Allstadt and Malone, 2014) and/or longer duration slip proportional to magnitude (Ekstrom et al., 2003). In addition, signals derived from glacial sources on volcanoes have often had a strongly repetitive nature which may persist on timescales of months to years (Jónsdóttir et al., 2009; Allstadt and Malone, 2014). This presents another overlap in characteristics with volcanic earthquakes since repetitive low frequency events associated with magma movement and failure have been documented prior to or during multiple eruptions (e.g. Iverson et al., 2006; Kendrick et al., 2014; Lamb et al., 2015). As an example for the potential issues of this confusion, careful analysis of seismic data revealed 150,000 low-magnitude ($M<1$), low-frequency repeating events at Mt. Rainier which were interpreted as caused by basal stick-slip motion beneath the glaciers on the volcano (Allstadt and Malone, 2014). The low-frequency and repetitive nature of these seismic events closely resembled seismicity often seen prior to or during eruptive activity at volcanoes around the world (Thelen et al., 2013). Therefore, the ability to distinguish between glacial and volcanic sources is vital for providing correct and rapid interpretations of seismicity at active glacier-clad volcanoes.

Here we present a detailed analysis of broadband seismic data collected at Llaima volcano during a temporary deployment in early 2015, with a primary focus on assessing the prevalence of icequakes. Llaima volcano is one of the most active volcanoes in Southern Chile and host to multiple glaciers on the upper flanks.This is the first known study to focus primarily on glacial seismic events on active volcanoes in Southern Chile. We detail several sequences of repetitive low-frequency seismic events at the volcano over the course of two months, and propose that these are of glacial rather than volcanic origin.

2 LLAIMA VOLCANO

Southern Chile is home to a chain of active ice-covered volcanoes, the most active of which is Llaima volcano (Fig. 1). Llaima is a complex stratovolcano and one of the largest in the region (377 km^3, 3179 m a.sl.; Völker et al., 2011) and largely composed of basaltic to andesitic composition lavas (de Maisonneuve et al., 2012). Up to 54 documented eruptions have occurred at the volcano since the 17th century (Naranjo and Moreno, 2005; Franco et al., 2019). The most recent episode, from 2007 to 2009, was the strongest since the 1950's with ash columns reaching 7 km above sea level and lahars generated by melting glacial ice (Franco et al., 2019).

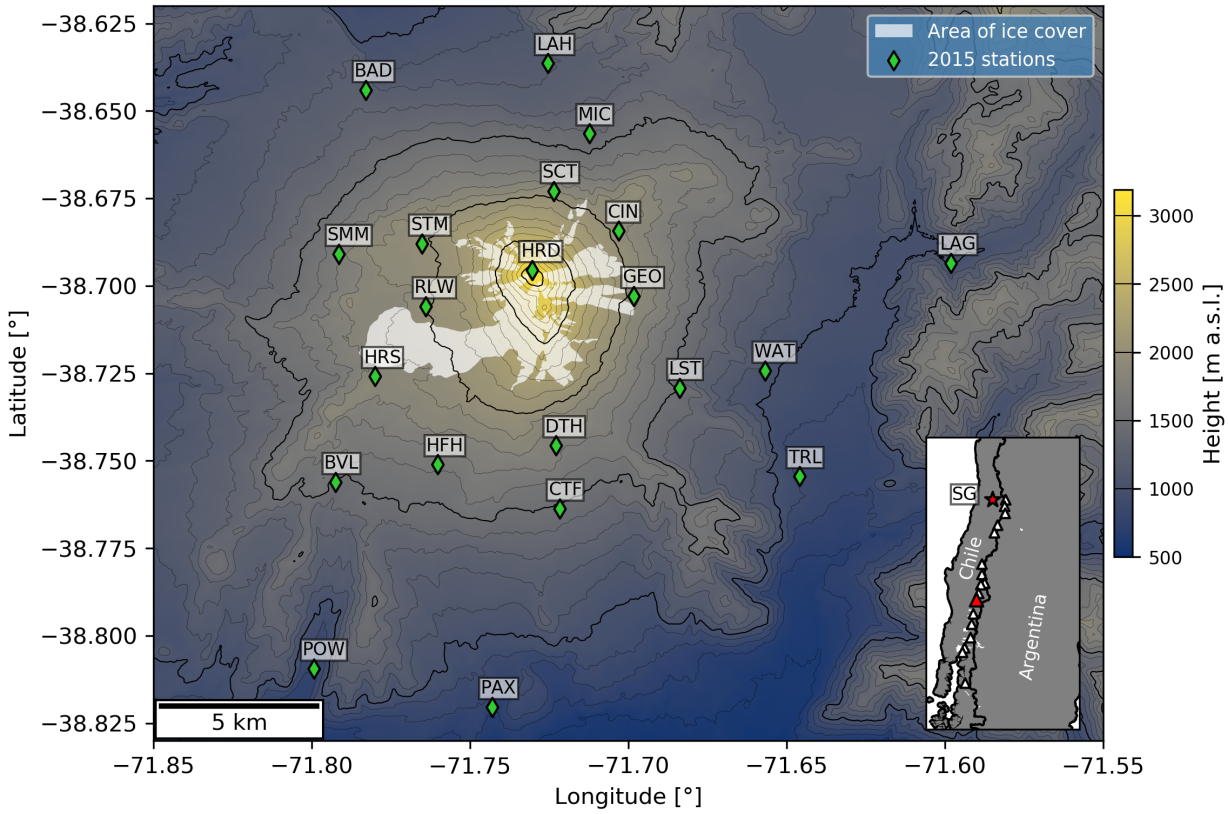

Figure 1. Map of Llaima volcano with the locations of the 2015 seismic stations used in this study marked with green diamonds (5 of the 26 stations are not visible). Also marked are the mapped summit glacial areas marked as 'clear' or 'debris-covered' ice (white area). Thick and thin contours mark 500 and 100 m altitude intervals, respectively. Inset: Map of Southern Chile with the location of Llaima volcano (red triangle) and Santiago (red star, SG) marked. Also plotted are the locations of other ice-covered volcanoes within the Southern Volcanic Zone of Chile that have displayed eruptive activity in last 200 years (white triangles; Venzke, 2013).

There remain difficulties in measuring the total glacial area on volcanoes due to extensive debris cover from eruptions as well as distinguishing between persistent snow patches and glacial ice. The glacial area presented in this study was calculated by using high-resolution satellite images taken on March 6 2016 (white area in Fig. 1). Areas of ice were classified as either 'clear ice', 'debris-covered ice', or 'unclear', and totaled 5.37, 8.85, and 8.17 km^2, respectively; this study will not use areas classified as 'unclear' to improve our confidence in the locations of glacial ice on the volcano. Our estimate of the total glacial area on Llaima volcano is significantly larger than 5.5 km^2 estimated by Reinthaler et al. (2019), but this value was calculated using lower resolution images in which debris-covered ice would not be clear. Nevertheless,

it is clear from satellite images that the glacial area at Llaima volcano has been significantly reduced in recent decades due to eruptive activity and global climate change (Reinthaler et al., 2019).

To provide a degree of security for nearby population centers, OVDAS (Observatorio Vulcanológico de los Andes Sur[1]) has deployed a network of stations around the volcano to continuously monitor its activity. OVDAS use the criteria described in Lahr et al. (1994); Chouet (1996), and Chouet and Matoza (2013) to identify and classify the earthquakes recorded by the seismic network around the volcano. Arrival times and waveform amplitudes are used to differentiate between volcanic and tectonic events. Using a reference station within the network, the volcanic earthquakes are classified as volcano-tectonic, long-period (including hybrid), or tremor events. Each type of earthquake has been associated with multiple distinct source mechanisms and relative temporal trends of each type has important implications for assessing the activity state of a volcano (see Chouet and Matoza, 2013, and references therein). OVDAS also manually distinguishes other non-volcanic or non-tectonic events such as cryogenic earthquakes, but have no mandate to track these events therefore little is known about their prevalence in the seismic record (Mora-Stock et al., 2014). Recent studies have attempted to construct automatic event classifiers for Llaima volcano using machine learning algorithms for pattern recognition with varying degrees of success (Curilem et al., 2014, 2018; Soto et al., 2018). However, these studies either grouped the few identified cryogenic earthquakes with other earthquake types (Curilem et al., 2014), or excluded them from their training databases (Curilem et al., 2018; Soto et al., 2018). There was no apparent recognition of the significant overlap and potential for confusion between glacially- and magmatically-derived earthquakes in the record. Before further automatic event classification algorithms are deployed for Llaima volcano, it is clear there exists a need to constrain the preponderance of cryogenic earthquakes in the seismic record.

2.1 2015 deployment

From January to March 2015, twenty-six broadband seismic stations were deployed across an approximately 30 x 20 km area centered on Llaima volcano as part of a UNC Chapel Hill, Boise State University and Southern Andes Volcano Observatory (OVDAS) collaboration (Fig. 1). Application of receiver function analysis to this seismic data revealed a low-velocity zone at 8-13 km depth beneath the volcano that could be interpreted as a magmatic body (Bishop et al., 2018). The network used a variety of broadband seismometers that used various digitizers recording the data at 100 samples per second, see Table S1 for specific details of what each station used.

3 GENERATING A CATALOG OF CANDIDATE ICEQUAKES

To detect candidate seismic events at Llaima volcano, we applied a multistation detection algorithm on seismic data collected from 1 February to 31 March 2015. Trigger times were extracted from multiple stations using a short-term average/long-term average algorithm (STA/LTA), on condition that an event was detected by $\geq$2 stations. Considering the low magnitude and strong attenuation noted for icequakes at other volcanoes (e.g. Allstadt and Malone, 2014), we used only the eight closest stations to the summit for this step (marked by a asterisk in Table S1). Seismic data were preprocessed with a bandpass filter of 0.5-10 Hz to improve the signal-to-noise ratio (SNR).

From the catalog of candidate triggers compiled by the multi-station detection algorithm, our next step was to find seismic events that were repetitive over the period of study. In order to reduce the computing load, we followed a similar methodology to that detailed by Allstadt and Malone (2014) who used an

[1] part of Servicio Nacional de Geología y Minería (SERNAGEOMIN)

algorithm modified from Carmichael (2013). The method uses unsupervised clustering of seismic events so the user does not need to define templates in order to detect repeating events. First, we cross-correlate every event with all other events within each day and group them into families, using a minimum cross-correlation coefficient of 0.7 to define two events as a match. For each event, we used the first 5 s of the waveform, sufficient to include the largest wave amplitudes while minimizing the contribution of background noise. Seismograms from station GEO were used to build the catalog, as this station had the highest number of detected events. Families of repeating waveforms were defined using a hierarchical clustering method similar to that used by Buurman and West (2013) and Lamb et al. (2015). Next, a median waveform stack is computed for each family of 2 events or more detected each day. Each stack is then compared to all other stacks across the whole time period to find larger, multi-day families. Finally, in order to ensure the repeating event catalog is as complete as possible we scan the entire time period with a stacked waveform from each multi-day family in order to find any events potentially missed in the previous steps. For this step, we used the super-efficient cross-correlation algorithm (SEC-C), a frequency domain method that optimizes computations using an overlap-add approach, vectorization, and fast normalization (Senobari et al., 2019).

4 RESULTS

4.1 Catalog of low-level seismic activity

Between 1 February and 31 March 2015, we detected 4,894 seismic events at Llaima volcano (dashed grey bars in Fig. 2a). This value is significantly larger than the 572 seismic events that were manually cataloged by OVDAS during the same time period (red dash-dot line in Fig. 2a). The OVDAS catalog includes 490 seismic events dominated by low-frequency volcanic events (a.k.a. long-period) and 82 surface activity such as avalanches (Fig. S1). Using the catalog of automatically detected events, we identified 1,134 repeating seismic events that were divided across 11 different families (Fig. 2a, c). Of the 490 events cataloged as long-period events, only 2 matched with detected repeating seismic events (Fig. S2). The largest of these families included 396 of these events, with repose intervals of 1 to 15 hours. The rate of daily seismic event rates, including repeating seismic events, are relatively continuous throughout the period of study with no obvious indications of cyclic activity or significant changes in rates. Weather data collected at a station situated in the town of Melipeuco (approximately 17 km SSE from the volcano summit) indicates no significant rainfall or temperature fluctuations in the area during the period of study.

4.2 Characteristics of repeating seismic events

The earthquakes allocated to the largest family of repeating events (henceforth called Family 1) are generally small, with magnitudes of less than 1, and appear to be of an emergent low-frequency nature (Fig. 3a). However, the low-frequency and emergent nature of these events were likely the result of path effects as the waves were strongly altered and attenuated as they traveled away from the volcano (Fig. 4a). To compare the relative magnitudes of events within the family, we calculate the pseudo-energy for each event waveform, which is the integral of the Hilbert envelope of the waveform (Rowe et al., 2002; Thelen et al., 2013). For Family 1, there is a very weak correlation between the repose interval between events and the pseudo-energy of the subsequent seismic event (Fig. 3b); this characteristic is not shared across most of the other families detected (Fig. S3). When events in each family are binned by time-of-day occurrence, there are few, if any, tangible correlations with time of day or with temperature (Fig. S4). However, it's likely that the families here do not contain enough events for any significant correlations to become visible .

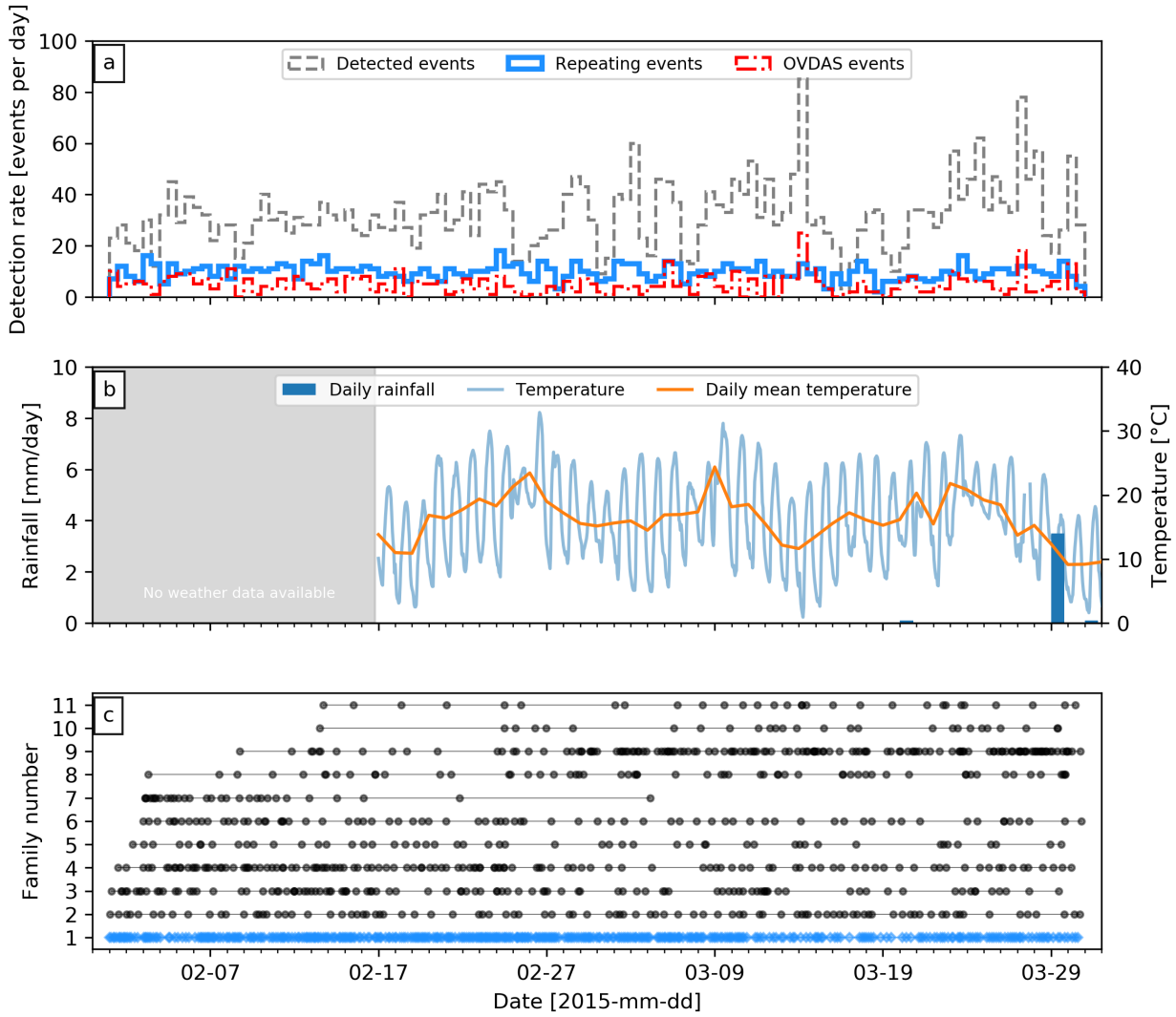

Figure 2. (a) Rates for events automatically detected (grey dashed bars), events classified as repeaters (red solid bars), and seismic events manually classified by OVDAS (red dashed bars) from 1 February to 31 March 2015 in 12-hour bins. (b) Daily events in rainfall (blue bars) and variations in temperature on an hourly (light blue) and daily rate (orange line). (c) Catalog of family occurrence in our dataset. Each plotted point represents the time of an event, and lines join events from the same family. The largest family (Family 1) is plotted using blue diamonds for the individual events.

4.3 Location of largest families

Calculating the source locations for each of the families is crucial for understanding the source mechanism(s) involved. However, locating individual events within each family detected at Llaima volcano without unacceptable error margins is impossible due to the emergent and low SNR nature of each waveform, as well as the rapid attenuation of the signal as it moves away from volcano (Fig. 4a). Nonetheless, following Allstadt and Malone (2014), we can take advantage of the repeating nature of these families and calculate median stacks for each family at each station. If there are enough events in the family, clearer signals with relatively high SNR can be acquired on at least 3 stations in the network (Fig. 4b). The improvement in the SNR is such that relative P-wave arrival times across the station can be used for a grid-search location algorithm. In addition, we can also determine the direction of first motions at ten

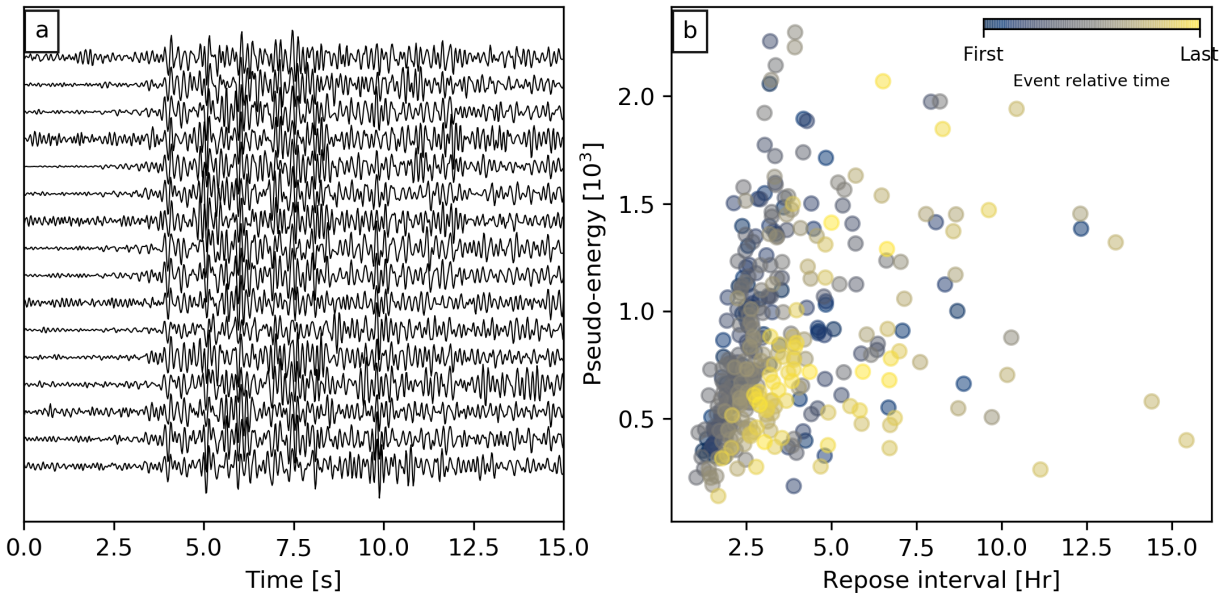

Figure 3. (a) Waveforms of the first 15 events in Family 1, as recorded at station GEO. (b) Repose intervals versus pseudo-energy for each event in Family 1, colored by their relative age within the family duration, using waveforms recorded at station GEO.

of the closest stations to the volcano summit for Family 1 (Fig. 5). The first motions for Family 1 in the vertical component show mixed polarities across these stations, indicating a shear motion component for the source mechanism. However, the stacking method only applied for three families, as the SNR did not improve enough for clear P-wave arrivals in the remaining families.

Once the P-wave arrival times were picked, we used a brute-force 3D grid-search algorithm to estimate source locations. This algorithm uses the relative arrival times between the first recorded arrival and all subsequent arrival times to find the most appropriate source location using a fixed P-wave velocity value. We defined the grid of source nodes using a 29 m horizontal and 37 m vertical resolution. A previous study used a seismic velocity of 2.5 kms^{-1} for the surface layer to calculate seismic power for continuous tremor recorded during the 2007-2009 eruptive period (Franco et al., 2019). A compilation of seismic velocity profiles for andesitic-basaltic volcanoes suggest that P-wave velocities range from approximately 0.5 kms^{-1} at the surface up to 6 kms^{-1} at 4 km depth (Lesage et al., 2018). Crustal models developed by OVDAS for several volcanoes, including Llaima volcano, use a seismic velocity of 4 kms^{-1} for the upper layer of the volcanic edifice. Therefore, for our grid search we used a fixed value of 4 kms^{-1}.

The locations of the three largest families from which we could get enough clear P-wave arrival times are plotted in Figure 6. The locations of each family is tightly clustered around the summit vent, near or beneath the top of the glaciers. The depths of each family is very shallow, on the order of 10's of meters. However, it is important to note that the uncertainties in these locations are very high due to a number of factors. The use here of a 1-D velocity model is likely not appropriate for what is a very heterogeneous edifice. Furthermore, any slight misalignment of waveforms during stacking will introduce errors to the picked P-wave arrival times at each station. Errors may also be introduced during the manual picking of the P-wave arrival times. Lastly, the spacial resolution used during the brute-force grid-search algorithm enforces a minimum in the expected errors of the locations. Therefore, the locations presented here are a rough approximation of the actual source locations. Nevertheless, it is clear from the waveform arrival

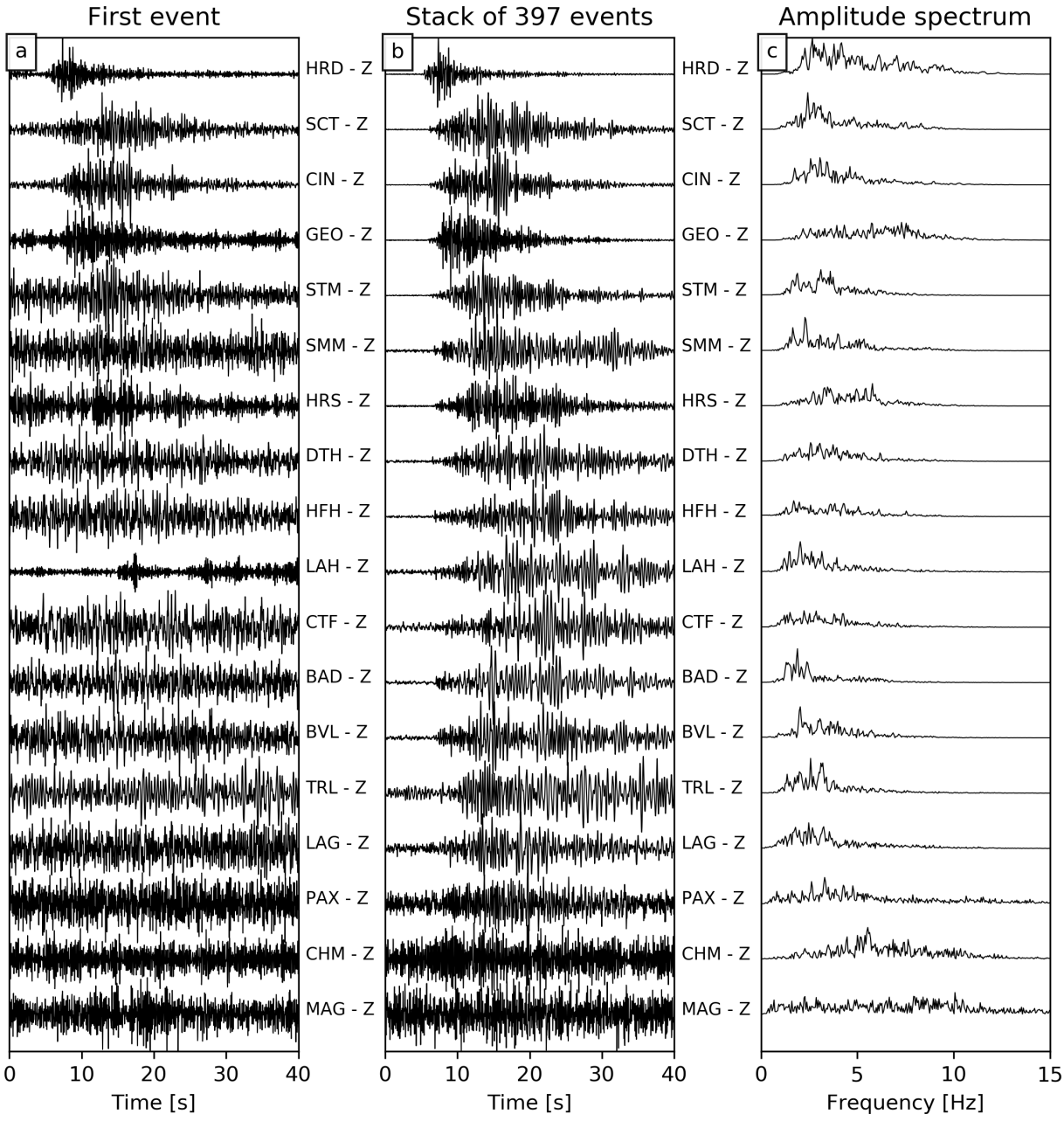

Figure 4. (a) The waveform of the first detected event in Family 1 as recorded at stations within the 2015 deployment, ordered by distance from the summit. (b) Stacked waveforms generated from the 397 events detected in Family 1 at each station. (c) Normalized frequency-amplitude spectra of the stack waveforms presented in panel (b).

195 times across the network (e.g. Family 1; Fig. 4a,b) that the source locations were nearest to station HRD
196 and therefore close to the volcano summit. For other families where not enough clear arrivals were acquired
197 to calculate locations, it is clear that some are located closer to station GEO instead of HRD (e.g. Family
198 3, 6 and 7; Fig. S6, S9, and S10, respectively). This indicates that the source locations for these familes
199 would be close to or beneath the termini of the mapped glacial areas in the east and north-east flanks of the
200 volcano.

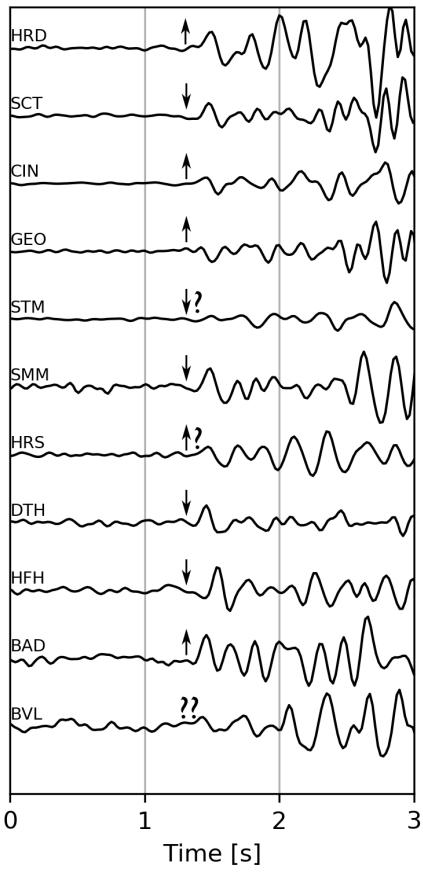

Figure 5. First arrivals of stacked waveforms of Family 1 as recorded by 11 stations in the 2015 network. Where the first motion is uncertain, they have been marked with question marks. The waveforms here have been manually realigned to approximately the same arrival time for the purpose of this plot.

4.4 Source locations over time

While it may not be possible to calculate exact source locations, coda wave interferometry (CWI) can use the repeating waveforms within each family to provide an estimate of source separation during the lifetime of the family (i.e. source location drift). Any migration in a repeating seismic source (or change in the seismic velocity properties of the medium) results in a change in distance (or velocity) to scatterers in the surrounding medium, which in turn affects the arrival times of phases in the waveform coda. Here we are assuming there was no change in the locations of scatterers in the medium. Allstadt and Malone (2014) used CWI to demonstrate drifts of up to 7 meters per day for the locations of repeating icequakes at Mt. Rainier volcano. Here, we use a similar approach on Family 1 to elucidate whether any drift may be occurring at the source location.

The correlation coefficient between waveforms, R, is related to the variance of the travel-time perturbation, σ_τ according to the following relationship (Snieder et al., 2002):

$$R = 1 - \frac{1}{2}\overline{\omega}^2\sigma_\tau^2 \tag{1}$$

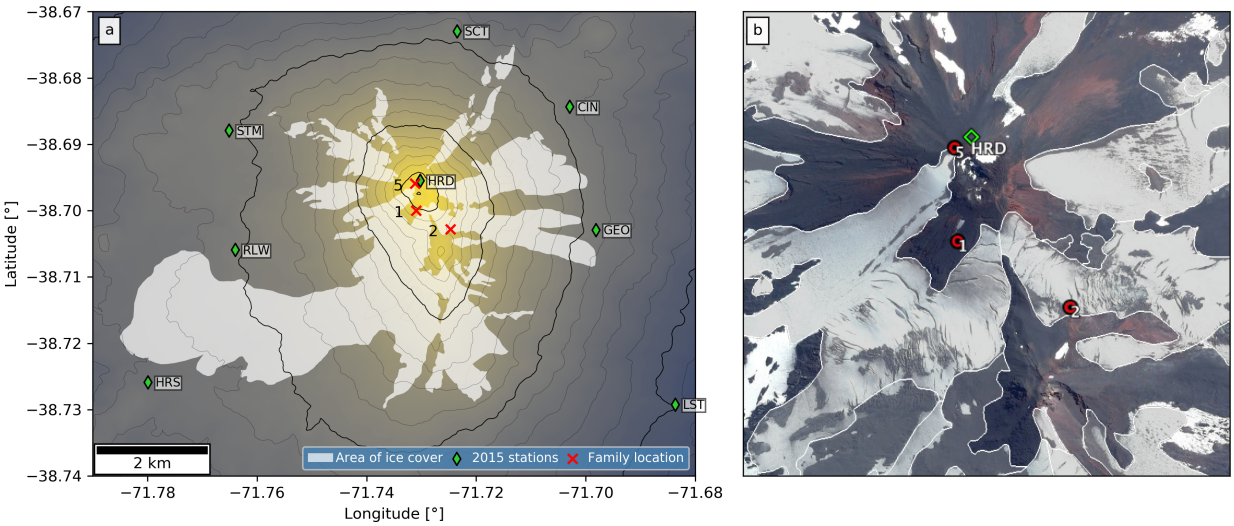

Figure 6. (a) Map of Llaima volcano summit area with the locations of the closest 2015 seismic stations used in this study marked with green diamonds. Also marked are the summit glacial areas (white area), as well as locations of three families (red crosses). Thick and thin contours mark 500 and 100 m altitude intervals, respectively. Colormap used is identical to that used in Fig. 1. (b) Satellite image of the summit area of Llaima volcano, with station HRD marked (green diamond) and the locations of the largest three families (red circles). Also marked are the mapped glacial areas (white areas). Image source: Google-CNRS-Airbus-Digital Globe, captured on March 6 2016.

where the frequency, $\overline{\omega}^2$, can be calculated from the seismogram data, $u(t)$:

$$\overline{\omega}^2 = \frac{\int_{t-T}^{t+T} \dot{u}^2(t')dt'}{\int_{t-T}^{t+T} u^2(t')dt'} \tag{2}$$

where the integral is performed over a window of length $2T$ centered at time t. We also apply a correcting factor to R to account for bias due to noise in the waveforms (Douma and Snieder, 2006). The relationship between the variance of the travel-time pertubation and inferred source migration depends on the source mechanism, such as explosive, point, or fault-plane (Snieder and Vrijlandt, 2005). Evidence from the mixed first-motion polarities (Fig. 5) suggest that it is reasonable to assume, for the purposes of this calculation, that the source is dominated by shear motion along a fault-plane. Therefore, if displacement occurs along a fault-plane, the source dislocation between waveforms, δ, is given by:

$$\delta = \left[7\left(\frac{2}{v_p^6} + \frac{3}{v_s^6}\right) / \left(\frac{6}{v_p^8} + \frac{7}{v_s^8}\right)\right]^{\frac{1}{2}} \sigma_\tau \tag{3}$$

where v_p and v_s are the P- and S-wave velocities in the medium. Note that using different seismic velocities or different source mechanisms will change the displacement magnitude, but not the pattern of movement over time. Lesage et al. (2018) compile measurements of v_p/v_s ratios for andesitic basaltic volcanoes that approximately range from 1.5 to 2.5. Here we calculate displacements using P-wave velocities ranging from 1 - 4 kms^{-1} , with a v_p/v_s ratio of 2. As the individual waveforms within Family 1 have relatively low SNR, we instead apply CWI to stacked subsets of the family in order to improve the SNR. Family 1, featuring 397 events, was divided up into 13 subsets of 30 or 31 events, and median stacks

were calculated from each stack. R was calculated using 8 second windows starting 5 s after the start of the stacked waveform, bandpass filtered at 1-10 Hz, for each stack relative to the first stack, and converted to δ.

For Family 1, the calculated displacements from waveforms recorded at two different stations (HRD, GEO) are $<$1 m/day (Fig. 7). The largest displacements appear to occur during the first part of the recorded family lifespan, before it stabilizes during the rest of the study period. Total source displacements at the highest v_p values used (4 kms^{-1}) are still significantly lower than what has been observed at other volcanoes (e.g. Mt. Rainier; Allstadt and Malone, 2014). While the displacements between each station may differ, the overall shape of the calculations are relatively similar which lends credibility to the calculations presented here.

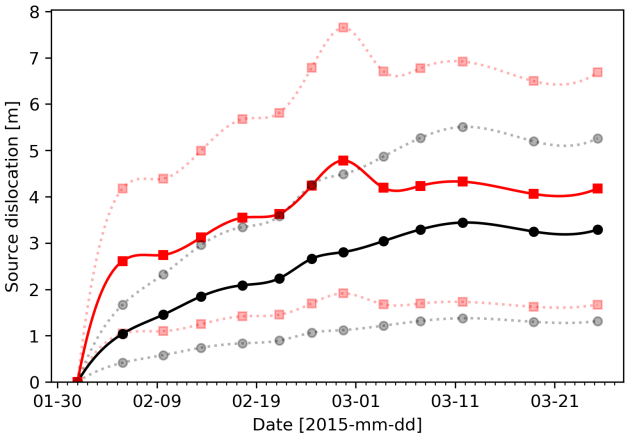

Figure 7. Calculated source displacements for Family 1 at stations GEO (black) and HRD (red). Solid lines are estimates using v_p of 2.5 kms^{-1} with dotted lines indicating the lower (1 kms^{-1}) and upper (4 kms^{-1}) bounds of possible seismic velocities.

5 DISCUSSION

Here we have presented results of analysis of broadband seismic data collected at Llaima volcano in 2015, with the aim of understanding the preponderance for icequake activity at the volcano. While previous studies have noted the presence of icequakes in the seismic record at the volcano (e.g. Curilem et al., 2014; Mora-Stock et al., 2014), they are apparently relatively rare compared to other ice-covered volcanoes (Métaxian et al., 2003; Jónsdóttir et al., 2009; Allstadt and Malone, 2014). Indeed, during our study period, OVDAS officially cataloged no icequakes as it is not within their mandate to do so (Fig. S1). While we study a relatively small time period, from our observations described above we would argue that glacially derived seismic events may be far more prevalent in the seismic record than previously thought.

We conclude that the low-frequency and repetitive seismic activity detailed here is caused by glacial movements on the flanks of Llaima volcano, for the following reasons: 1) No volcanic activity was observed at the volcano during the study period, and not since 2010. Therefore, no volcanically related source mechanisms can be inferred. 2) Despite only looking at two months of seismic data, it is clear that the repetitive families are persistent and long-lasting, which might be expected for glacially derived seismic events (e.g. Jónsdóttir et al., 2009; Allstadt and Malone, 2014). 3) The waveforms seen here share many characteristics as previously described icequakes at other volcanoes, i.e. low-amplitude, rapid attenuation.

4) The locations for three of the families, including the largest, place them close to or beneath glaciers near the summit of the volcano.

There exist other potential sources for low-frequency seismicity at volcanoes that are not directly related to magmatic activity or glacial movement. The movement of hydrothermal fluids through the system could possibly generate low-frequency seismicity of the kind described here (e.g. Rust et al., 2008). Indeed, persistent fumarolic activity is often observed close to, or within the summit vent of Llaima. However, this source mechanism cannot generate the high-frequency waveforms often seen at stations closest to the source (e.g. station HRD in Fig. 4). Alternatively, slow-slip failure through volcanic material at shallow depths can also generate seismic activity with a high- to low-frequency attenuation pattern (Bean et al., 2013). Temporally complex deformation was noted on the eastern flank of Llaima volcano prior to or during the 2007-09 eruption, and was inferred to be a result of a potential slow-slip landslide (Fournier et al., 2010).The location of this landslide (approximately 5 km east of station GEO) does not correlate with the locations calculated for the largest families here (Fig. 6) and there have been no studies detailing if deformation in this area had continued up to 2015. However, with the evidence presented here we cannot completely rule out shallow slow-slip as a potential source of minor seismic activity on other regions of the volcano.

For glacial sources of seismicity, there are multiple different mechanisms that have been documented (Podolskiy and Walter, 2016). We can disregard mechanisms involving hydraulic resonance in or below the ice (e.g. Lawrence and Qamar, 1979; Métaxian et al., 2003) because there are no consistent spectral peaks between stations or evidence of harmonics (Fig. 4c), though the resonant character of the signal could be lost due signal alteration in the heterogeneous medium at shallow depths. Furthermore, we observe mixed polarity first motions (Fig. 5) when hydraulic motion might be expected to generate isotropic first motion. For this reason, we also disregard mechanisms involving ice-fall or serac collapses (e.g. Jónsdóttir et al., 2009) as the impact of ice onto ground should not be expected to generate mixed polarity first motions. Besides, there are no well documented areas on the glacial ice at Llaima volcano that could host persistent, highly-repetitive ice-fall that could generate the seismic families documented here. Glacial crevassing is the most common type of alpine glacier seismic source (e.g. Neave and Savage, 1970; Walter et al., 2008), and has been documented to generate families of repeating events (e.g. Mikesell et al., 2012). However, this mechanism generates relatively little seismic energy and steep alpine glaciers tend to be poorly coupled to the bedrock (Kamb, 1970), so seismic waves are inefficiently transferred from ice to rock (Weaver and Malone, 1979). As a result, crevassing seismicity are usually only detected by seismic instruments deployed directly onto the ice or on rock in close proximity to the glacier (Weaver and Malone, 1979; Thelen et al., 2013). Again, the mixed polarity first motions present a strong argument against crevassing as it is a volumetric source and should generate isotropic first motions. It is worth noting that our analytical workflow made a key assumption that most of the icequakes that could be occurring at Llaima are of a repetitive and persistent nature. It is possible that there were also many small, non-repetitive seismic events of a glacial origin that were not automatically detected here. Outside of manually and painstakingly picking these possible events from the seismic record, it is not yet feasible to build a catalog of these events.

Of all the candidate source mechanisms, basal stick-slip sliding close to or at the interface between ice and rock is the most likely. Repetitive, low-frequency seismicity generated by discrete glacial movements along the base has been well documented (e.g. Weaver and Malone, 1976, 1979; Ekstrom et al., 2003; Caplan-Auerbach and Huggel, 2007; Zoet et al., 2012; Thelen et al., 2013; Allstadt and Malone, 2014). The repetitive, persistent families observed at Llaima volcano (Fig. 2c) require non-destructive and repeatable sources, which can be provided by stick-slip motion over a stationary asperity at the ice-rock interface.

Alternatively, stick-slip motion can also be generated by rocks embedded in the ice (i.e. 'dirty patch'; e.g. Allstadt and Malone, 2014) but the low or stationary motion of the source calculated from CWI (Fig. 7) suggests the former is more likely. The mixed polarity first motions for Family 1 (Fig. 5) are also consistent with shear failure at the source, in agreement with what is inferred to occur during stick-slip motion. Stick-slip behavior requires two conditions be met: 1) friction must decrease with slip velocity, so that the associated acceleration can be sustained, and 2) healing (i.e. strengthening) must occur at the slip interface, so that static stress can be recharged (Zoet and Iverson, 2018). With the latter condition, one effect is that longer time periods without slip would lead to bigger stress build-up and bigger subsequent seismic events, a behavior that is hinted at for Family 1 (Fig. 3b). However, other laboratory experiments have shown that temperature changes can have a significant effect on the strength and stability of ice-on-rock friction (McCarthy et al., 2017). This may explain why we find a weak correlation between the repose interval and the pseudo-energies of the events in Family 1 (Fig. 3b) and very little correlation in the other families (Fig. S3). Laboratory experiments have shown that stick-slip behavior can occur in soft-bedded glaciers (Zoet and Iverson, 2018), which may be a condition beneath the glaciers at Llaima and other ice-covered volcanoes due to eruptive products such as tephra.

Llaima volcano has had at least two permanent seismic stations for monitoring activity since 2006, with more stations added during and after the 2007-09 eruptive episode (Franco et al., 2019). Why have the sequences of low-frequency, low-amplitude families described here not been detailed in previous work or in the OVDAS seismic catalog for the volcano? While icequakes have long been noticed in the seismic record at Llaima volcano, limited resources and time have meant that priority has been given to cataloging only volcanic or nearby tectonic events. Nevertheless, it is likely that the low-energy nature of these seismic events would mean they had relatively high SNR at the permanent stations, thus would be too small to be noticed during manual inspection of the seismic data. This is reflected in the fact that only 2 of the 'long-period' events cataloged by OVDAS during this time period matched with detected repeating seismic events (Fig. S2). There is currently no program for automatically searching for repeating seismic events at Llaima, although there are tools currently available or in development for such a use (e.g. REDPy; Hotovec-Ellis and Jeffries, 2016). Longer-term studies have found high variability in the number of icequakes at volcanoes, that often relate to observable changes in glacial behavior or seasonal changes in snow loading or temperature (e.g. Weaver and Malone, 1979; Allstadt and Malone, 2014). These studies also noted that the base of a glacier is a dynamic environment with some time periods more favorable for basal stick-slip behavior than other time periods. Thus, there is a good chance that the seismic station network deployed in early 2015 were coincidentally in the right place at the right time to detect the icequakes at Llaima volcano. As this study only looks at a relatively short two month period at the volcano, it is clear there is a need to expand the analysis to a multi-year scale so that seasonal changes in glacial seismic activity can be constrained. Furthermore, the locations calculated here would be of an unacceptably low quality for the needs of continuous monitoring and risk assessment. Therefore, future deployments at Llaima will need to explore new deployment configurations around the glaciers to help constrain the source locations for such low energy events.

The findings detailed in this study have important implications for continuous monitoring at Llaima volcano and other ice-covered volcanoes in Chile. At the time of writing, there are at least 8 permanent broadband seismic stations deployed around Llaima volcano which are collectively producing a significant geophysical dataset. This is one such example of an ever-growing volume of geophysical data that require the design and implementation of efficient tools capable of detecting all signals of interest, particularly immediately prior to eruptive activity. Several studies have designed and tested pattern recognition and machine learning tools for discriminating seismic signals at Llaima volcano, with varying degrees of

success (Curilem et al., 2014, 2018). However, these algorithms have been 'trained' using seismic catalogs that did not account for the significant overlap in characteristics between low-frequency volcanic signals and glacial events. The observations presented in this study raise the possibility that a significant number of events that were classified as volcanic were actually glacial in origin. Therefore, before new automatic algorithms are developed for seismic data at ice-covered volcanoes, more work is needed to efficiently separate the seismic events of glacial and volcanic origin.

6 CONCLUSIONS

Glacially derived seismic events, or icequakes, can share many characteristics used to define low-frequency volcanic earthquakes. Thus, there is a present need to improve our ability for distinguishing between these types of seismic events at active ice-covered volcanoes. Here we present a detailed analysis of two months of broadband seismic data collected at Llaima volcano in early 2015, one of the largest and most active ice-covered volcanoes in Chile. The aim of this analysis was to establish the quantity, characteristics, and locations of any glacially derived seismic events that may have occurred. We detail the presence of at least 11 families of repeating seismic events of a low-frequency, low-amplitude nature, the largest of which contained 397 events. Through stacking of waveforms in each family, we are able to calculate approximate locations for 3 of the largest families and results suggest they are located at shallow depths beneath glacial areas around the summit vent. Characteristics of the largest family, particularly the repose interval versus pseudo-energy relation and the mixed polarity first motion arrivals, lead us to conclude that these events were derived from stick-slip motion along the base of a glacier near the summit of the volcano. This study represents the first documented attempt at beginning to quantify the prevalence of icequakes at ice-covered volcanoes in Southern Chile. The observations presented here have clear implications for future studies of volcano-seismicity at Llaima volcano and other ice-covered active volcanoes in Southern Chile. However, these observations are derived from a relatively short time interval (2 months) compared to previous studies of icequakes at other volcanoes which used over a decade of seismic data (Jónsdóttir et al., 2009; Allstadt and Malone, 2014). It is clear there is a need to build on this study by expanding the analysis across the whole seismic archive from not only Llaima volcano, but other ice-covered volcanoes in Southern Chile.

AUTHOR CONTRIBUTIONS

ODL carried out the calculation and analysis, and drafted the manuscript. JML helped with the location calculation. LFM and JL provided OVDAS catalog data and weather data. AR provided the data to quantify the location and amount of glacial ice on Llaima. SJL and MJS participated in the design of the study. All authors read and approved the final manuscript.

ACKNOWLEDGMENTS

This research was performed while ODL held an NRC Research Associateship with the U.S. Army Research Laboratory/Army Research Office while based at the University of North Carolina at Chapel Hill. The authors wish to thank Rebecca Rodd for help with field data collection and deployment organization in 2015, as well as to Jeffrey B. Johnson, Timothy J. Ronan, and Thomas L. Otheim for their help in the fieldwork. JML acknowledges the support from NSF grants CDI 1125185 and AGS-1551999.

DATA AVAILABILITY STATEMENT

All data presented here will be made available on request to the corresponding author.

REFERENCES

Allstadt, K. E. and Malone, S. D. (2014). Swarms of repeating stick-slip icequakes triggered by snow loading at Mount Rainier volcano. *Journal of Geophysical Research: Earth Surface* 119, 1180–1203. doi:10.1002/2014JF003086

Aster, R. C. and Winberry, J. P. (2017). Glacial seismology. *Reports on Progress in Physics* 80. doi:10.1088/1361-6633/aa8473

Bean, C. J., De Barros, L., Lokmer, I., Métaxian, J.-P., O' Brien, G., Murphy, S., et al. (2013). Long-period seismicity in the shallow volcanic edifice formed from slow-rupture earthquakes. *Nature Geoscience* 7, 71–75. doi:10.1038/ngeo2027

Bishop, J., Lees, J., Biryol, C. B., Mikesell, T. D., and Franco, L. (2018). Examining the interior of Llaima Volcano with receiver functions. *Journal of Volcanology and Geothermal Research* 352, 1–9. doi:10.1016/j.jvolgeores.2017.11.022

Buurman, H. and West, M. E. (2013). Magma fracture and hybrid earthquakes in the conduit of Augustine Volcano. *Geophysical Research Letters* 40, 6038–6042. doi:10.1002/2013GL057864

Caplan-Auerbach, J. and Huggel, C. (2007). Precursory seismicity associated with frequent, large ice avalanches on Iliamna volcano, Alaska, USA. *Journal of Glaciology* 53, 128–140. doi:10.3189/172756507781833866

Carmichael, J. D. (2013). *Melt-triggered seismic response in hydraulically-active polar ice: Observations and methods*. Phd thesis, University of Washington

Chouet, B. A. (1996). Long-period volcano seismicity: its source and use in eruption forecasting. *Nature* 380, 309–316. doi:10.1038/380309a0

Chouet, B. A. and Matoza, R. S. (2013). A multi-decadal view of seismic methods for detecting precursors of magma movement and eruption. *Journal of Volcanology and Geothermal Research* 252, 108–175. doi:10.1016/j.jvolgeores.2012.11.013

Curilem, M., Huenupan, F., Beltrán, D., San Martin, C., Fuentealba, G., Franco, L., et al. (2014). Pattern recognition applied to seismic signals of Llaima volcano (Chile): An evaluation of station-dependent classifiers. *Journal of Volcanology and Geothermal Research* 282, 134–147. doi:10.1016/j.jvolgeores.2016.02.006

Curilem, M., Mello, R., Huenupan, F., San Martin, C., Franco, L., Hernández, E., et al. (2018). Discriminating seismic events of the Llaima volcano (Chile) based on spectrogram cross-correlations. *Journal of Volcanology and Geothermal Research* 367, 63–78. doi:10.1016/J.JVOLGEORES.2018.10.023

de Maisonneuve, C. B., Dungan, M. A., Bachmann, O., and Burgisser, A. (2012). Insights into shallow magma storage and crystallization at Volcán Llaima (Andean Southern Volcanic Zone, Chile). *Journal of Volcanology and Geothermal Research* 211-212, 76–91. doi:10.1016/j.jvolgeores.2011.09.010

Douma, H. and Snieder, R. (2006). Correcting for bias due to noise in coda wave interferometry. *Geophysical Journal International* 164, 99–108. doi:10.1111/j.1365-246X.2005.02807.x

Ekstrom, G., Nettles, M., and Abers, G. A. (2003). Glacial Earthquakes. *Science* 302, 622–624. doi:10.1126/science.1088057

Fournier, T. J., Pritchard, M. E., and Riddick, S. N. (2010). Duration, magnitude, and frequency of subaerial volcano deformation events: New results from Latin America using InSAR and a global synthesis. *Geochemistry, Geophysics, Geosystems* 11. doi:10.1029/2009GC002558

Franco, L., Palma, J. L., Lara, L. E., Gil-Cruz, F., Cardona, C., Basualto, D., et al. (2019). Eruptive sequence and seismic activity of Llaima volcano (Chile) during the 2007–2009 eruptive period: Inferences of the magmatic feeding system. *Journal of Volcanology and Geothermal Research* 379, 90–105. doi:10.1016/j.jvolgeores.2019.04.014

Hotovec-Ellis, A. J. and Jeffries, C. (2016). Near Real-time Detection, Clustering, and Analysis of Repeating Earthquakes: Application to Mount St. Helens and Redoubt Volcanoes. In *Seismological Society of America Annual Meeting*

Iverson, R. M., Dzurisin, D., Gardner, C. A., Gerlach, T. M., LaHusen, R. G., Lisowski, M., et al. (2006). Dynamics of seismogenic volcanic extrusion at Mount St Helens in 2004-05. *Nature* 444, 439–43. doi:10.1038/nature05322

Jónsdóttir, K., Roberts, R., Pohjola, V., Lund, B., Shomali, Z. H., Tryggvason, A., et al. (2009). Glacial long period seismic events at Katla volcano, Iceland. *Geophysical Research Letters* 36, L11402. doi:10.1029/2009GL038234

Kamb, B. (1970). Sliding motion of glaciers: Theory and observation. *Reviews of Geophysics* 8, 673. doi:10.1029/RG008i004p00673

Kendrick, J. E., Lavallée, Y., Hirose, T., Di Toro, G., Hornby, A. J., De Angelis, S., et al. (2014). Volcanic drumbeat seismicity caused by stick-slip motion and magmatic frictional melting. *Nature Geoscience* 7, 438–442. doi:10.1038/NGEO2146

Lahr, J. C., Chouet, B. A., Stephens, C. D., Power, J. A., and Page, R. A. (1994). Earthquake classification, location, and error analysis in a volcanic environment: implications for the magmatic system of the 1989-1990 eruptions at Redoubt Volcano, Alaska. *Journal of Volcanology and Geothermal Research* 62, 137–151

Lamb, O. D., De Angelis, S., Umakoshi, K., Hornby, A. J., Kendrick, J. E., and Lavallée, Y. (2015). Repetitive fracturing during spine extrusion at Unzen volcano, Japan. *Solid Earth* 6, 1277–1293. doi:10.5194/se-6-1277-2015

Lawrence, W. S. and Qamar, A. (1979). Hydraulic Transients: A Seismic Source in Volcanoes and Glaciers. *Science* 203, 654–656. doi:10.1126/science.203.4381.654

Lesage, P., Heap, M. J., and Kushnir, A. (2018). A generic model for the shallow velocity structure of volcanoes. *Journal of Volcanology and Geothermal Research* 356, 114–126. doi:10.1016/j.jvolgeores.2018.03.003

McCarthy, C., Savage, H., and Nettles, M. (2017). Temperature dependence of ice-on-rock friction at realistic glacier conditions. *Philosophical Transactions of the Royal Society A: Mathematical, Physical and Engineering Sciences* 375, 20150348. doi:10.1098/rsta.2015.0348

Métaxian, J.-P., Araujo, S., Mora, M. M., and Lesage, P. (2003). Seismicity related to the glacier of Cotopaxi Volcano, Ecuador. *Geophysical Research Letters* 30, 1–4. doi:10.1029/2002GL016773

Mikesell, T. D., Wijk, K. V., Haney, M. M., Bradford, J. H., Marshall, H. P., and Harper, J. T. (2012). Monitoring glacier surface seismicity in time and space using Rayleigh waves. *Journal of Geophysical Research* 117, 1–12. doi:10.1029/2011JF002259

Mora-Stock, C., Thorwart, M., Wunderlich, T., Bredemeyer, S., Hansteen, T. H., and Rabbel, W. (2014). Comparison of seismic activity for Llaima and Villarrica volcanoes prior to and after the Maule 2010 earthquake. *International Journal of Earth Sciences* 103, 2015–2028. doi:10.1007/s00531-012-0840-x

458 Naranjo, J. A. and Moreno, H. (2005). Geología del Volcán Llaima. *Carta Geológica de Chile - Serie*
459 *Geología Básica* 88, 1–37
460 Neave, K. G. and Savage, J. C. (1970). Icequakes on the Athabasca Glacier. *Journal of Geophysical*
461 *Research* 75, 1351–1362. doi:10.1029/JB075i008p01351
462 Neuberg, J. W., Tuffen, H., Collier, L., Green, D. N., Powell, T., and Dingwell, D. B. (2006). The trigger
463 mechanism of low-frequency earthquakes on Montserrat. *Journal of Volcanology and Geothermal*
464 *Research* 153, 37–50. doi:10.1016/j.jvolgeores.2005.08.008
465 Podolskiy, E. A. and Walter, F. (2016). Cryoseismology. *Reviews of Geophysics* S4, 708–758. doi:10.
466 1002/2016RG000526
467 Reinthaler, J., Paul, F., Granados, H. D., Rivera, A., and Huggel, C. (2019). Area changes of glaciers
468 on active volcanoes in Latin America between 1986 and 2015 observed from multi-temporal satellite
469 imagery. *Journal of Glaciology* , 1–15doi:10.1017/jog.2019.30
470 Rowe, C. A., Aster, R. C., Borchers, B., and Young, C. J. (2002). An Automatic, Adaptive Algorithm for
471 Refining Phase Picks in Large Seismic Data Sets. *Bulletin of the Seismological Society of America* 92,
472 1660–1674
473 Rust, A. C., Balmforth, N. J., and Mandre, S. (2008). The feasibility of generating low-frequency volcano
474 seismicity by flow through a deformable channel. *Geological Society, London, Special Publications* 307,
475 45–56. doi:10.1144/SP307.4
476 Senobari, N. S., Funning, G. J., Keogh, E., Zhu, Y., Yeh, C. M., Zimmerman, Z., et al. (2019). Super-
477 Efficient Cross-Correlation (SEC-C): A Fast Matched Filtering Code Suitable for Desktop Computers.
478 *Seismological Research Letters* 90, 322–334. doi:10.1785/0220180122
479 Snieder, R., Gret, A., Douma, H., and Scales, J. (2002). Coda Wave Interferometry Estimating Nonlinear
480 Behaviour in Seismic Velocity. *Science* 295, 2253–2255. doi:10.1126/science.1070015
481 Snieder, R. and Vrijlandt, M. (2005). Constraining the source separation with coda wave interferometry:
482 Theory and application to earthquake doublets in the Hayward fault, California. *Journal of Geophysical*
483 *Research* 110, 2156–2202. doi:10.1029/2004JB003317
484 Soto, R., Huenupan, F., Meza, P., Curilem, M., and Franco, L. (2018). Spectro-temporal features applied
485 to the automatic classification of volcanic seismic events. *Journal of Volcanology and Geothermal*
486 *Research* 358, 194–206. doi:10.1016/j.jvolgeores.2018.04.025
487 Thelen, W. A., Allstadt, K. E., De Angelis, S., Malone, S. D., Moran, S. C., and Vidale, J. (2013). Shallow
488 repeating seismic events under an alpine glacier at Mount Rainier, Washington, USA. *Journal of*
489 *Glaciology* 59, 345–356. doi:10.3189/2013JoG12J111
490 Venzke, E. (2013). *Global Volcanism Program*. doi:10.5479/si.GVP.VOTW4-2013
491 Völker, D., Kutterolf, S., and Wehrmann, H. (2011). Comparative mass balance of volcanic edifices at the
492 southern volcanic zone of the Andes between 33°S and 46°S. *Journal of Volcanology and Geothermal*
493 *Research* 205, 114–129. doi:10.1016/j.jvolgeores.2011.03.011
494 Walter, F., Deichmann, N., and Funk, M. (2008). Basal icequakes during changing subglacial water
495 pressures beneath Gornergletscher, Switzerland. *Journal of Glaciology* 54, 511–521. doi:10.3189/
496 002214308785837110
497 Weaver, C. S. and Malone, S. D. (1976). Mt. Saint Helens Seismic Events: Volcanic Earthquakes or Glacial
498 Noises? *Geophysical Research Letters* 3, 197–200
499 Weaver, C. S. and Malone, S. D. (1979). Seismic Evidence for Discrete Glacier Motion at the Rock–Ice
500 Interface. *Journal of Glaciology* 23, 171–184. doi:10.1017/S0022143000029816
501 West, M. E., Larsen, C. F., Truffer, M., O'Neel, S., and LeBlanc, L. (2010). Glacier microseismicity.
502 *Geology* 38, 319–322. doi:10.1130/G30606.1

Zoet, L. K., Anandakrishnan, S., Alley, R. B., Nyblade, A. A., and Wiens, D. A. (2012). Motion of an Antarctic glacier by repeated tidally modulated earthquakes. *Nature Geoscience* 5, 623–626. doi:10.1038/ngeo1555

Zoet, L. K. and Iverson, N. R. (2018). A healing mechanism for stick-slip of glaciers. *Geology* 46, 807–810. doi:10.1130/G45099.1